



Article

Towards Improved Satellite Data Utilization in China: Insights from an Integrated Evaluation of GSMaP-GNRT6 in Rainfall Patterns

Zunya Wang ^{1,*} and Qingquan Li ^{1,2}

¹ China Meteorological Administration Key Laboratory for Climate Prediction Studies, National Climate Center, Beijing 100081, China; liqq@cma.gov.cn

² Collaborative Innovation Center on Forecast and Evaluation of Meteorological Disasters, Nanjing University of Information Science & Technology, Nanjing 210044, China

* Correspondence: wangzy@cma.gov.cn

Abstract: To improve the utilization of satellite-based data and promote their development, this analysis comprehensively evaluates the performance of GSMaP Near-real-time Gauge-adjusted Rainfall Product version 6 (GSMaP_GNRT6) data in depicting precipitation over China from 2001 to 2020 by comparing four precipitation indices—accumulated precipitation, number of rainy days and rainstorm days, and precipitation maxima—with daily precipitation data from 2419 stations across China on monthly and annual time scales. The results show that the GSMaP-GNRT6 data effectively capture the overall spatial pattern of the four precipitation indices, but biases in the spatial distribution of the number of rainy days from July to September and the precipitation maxima during the wintertime are evident. A general underestimation of GSMaP-GNRT6 data is observed in the average for China. The annual precipitation amount, the number of rainy days and rainstorm days, and the precipitation maxima based on the GSMaP-GNRT6 data are 17.6%, 35.5%, 31.6% and 11.8% below the station observations, respectively. The GSMaP-GNRT6 data better depict the precipitation in eastern China, with the errors almost halved. And obvious overestimation of the number of rainstorm days and precipitation maxima occurs in western China, reaching up to 60%. Regarding the accumulated precipitation, the number of rainstorm days and the precipitation maxima, the GSMaP-GNRT6 data show an almost consistent interannual variation and increasing trends that are consistent with the station observations. However, the magnitude of the increasing trend based on the GSMaP-GNRT6 data is larger, especially at the beginning of the 21st century. Conversely, a considerable discrepancy in the annual variation and an almost opposite trend can be observed in the number of rainy days between the GSMaP-GNRT6 data and the station observations.

Keywords: GSMaP-GNRT6; station observations; validation; precipitation; rainy days; rainstorm days; precipitation maxima



Citation: Wang, Z.; Li, Q. Towards Improved Satellite Data Utilization in China: Insights from an Integrated Evaluation of GSMaP-GNRT6 in Rainfall Patterns. *Remote Sens.* **2024**, *16*, 755. <https://doi.org/10.3390/rs16050755>

Academic Editor: Yuriy Kuleshov

Received: 4 January 2024

Revised: 9 February 2024

Accepted: 18 February 2024

Published: 21 February 2024



Copyright: © 2024 by the authors. Licensee MDPI, Basel, Switzerland. This article is an open access article distributed under the terms and conditions of the Creative Commons Attribution (CC BY) license (<https://creativecommons.org/licenses/by/4.0/>).

1. Introduction

Precipitation is one of the most important meteorological elements. As an integral part of the global water and energy cycle, it is not only an indicator of the prevailing local weather and climate conditions, but also has the potential to trigger meteorological disasters. Excessive precipitation leads to flooding, mudslides, urban inundation and waterlogging [1–7], while insufficient precipitation invariably results in drought [8–12]. Floods and droughts have significant negative impacts on agriculture, the economy and even human safety [13–18]. Especially against the background of global warming, the intensity and frequency of precipitation extremes have greatly increased, causing severe damage to society worldwide [15,19–23]. As precipitation monitoring is crucial for weather forecasting and climate prediction, as well as for disaster prevention and mitigation, precipitation estimation is a major challenge [24–32].

Station observations are one of the most important methods for precipitation monitoring due to their high accuracy and real-time capability. However, the spatial resolution and homogeneity of meteorological monitoring is limited by the scattered distribution of observations [31,33,34]. With the progress of satellite remote sensing technology, the corresponding data are widely utilized. On the one hand, satellite remote sensing data are used to create reanalysis datasets [35,36]. In particular, two NCEP/NCAR reanalysis datasets (NCEP1 and NCEP2) [37,38], the reanalysis data of the European Centre for Medium-Range Weather Forecasts (ECMWF) (ERA-40, ERA-Interim and ERA5) [39–42], the NCEP Climate Forecast System Reanalysis System (CFSR) [43,44] and the Japanese 55-year Reanalysis (JRA-55) [45,46] are widely used. On the other hand, satellite observations can also provide meteorological monitoring with high spatial resolution and wide spatial coverage. Currently, various satellite precipitation datasets are available, such as the NOAA Climate Data Record (CDR) of the CPC Morphing Technique (CMORPH) [47], the Tropical Rainfall Measuring Mission (TRMM) Multi-Satellite Precipitation Analysis (TMPA) [48], Precipitation Estimation from Remotely Sensed Information using Artificial Neural Networks (PERSIANN) [49–51], Global Satellite Mapping of Precipitation (GSMaP) [52,53] and others. In order to improve the application of satellite precipitation, a number of validation and evaluation studies have been carried out. Global and regional precipitation, especially precipitation extremes, have been compared in numerous studies [32,33,46,54–56]. These studies report on the general spatial and temporal consistency and discuss the advantages and limitations of gauge-based precipitation, satellite estimates and reanalysis data.

The GSMaP was developed by the Japan Aerospace Exploration Agency (JAXA) [46,53], under the framework of the Global Precipitation Measurement (GPM), an international collaboration aimed at achieving highly accurate and frequent global precipitation observations [57,58]. GSMaP provides global precipitation estimates with a temporal resolution as high as 1 h and a horizontal resolution of 0.1° . Its reliability has been extensively evaluated in various regions, such as Japan [53,59], the United States [53,60], Mainland China [61–64], Australia [65] and Indonesia [66]. These studies demonstrate the primary accuracy of GSMaP and highlight biases in spatial distribution and magnitude in the climatology of daily or seasonal precipitation. To improve the monitoring of extreme precipitation, the World Meteorological Organization (WMO) initiated the Space-Based Weather and Climate Extremes Monitoring (SWCEM) and a two-year (2018–2019) demonstration project, known as the WMO Space-Based Weather and Climate Extremes Monitoring Demonstration Project (SEM DP), conducted in the East Asia and Western Pacific region [67]. In this project, the generally good skill of GSMaP in monitoring extreme wet and dry events is validated through various case studies.

Despite the relatively abundant research on the validation of the GSMaP data, additional efforts are still required to address the shortcomings in the current investigation. On the one hand, existing outcomes are predominantly derived from case studies or short-term records, necessitating verification through more extended-term datasets. On the other hand, previous research has predominantly focused on climatology and daily or seasonal rainfall amounts, overlooking aspects such as climate variations and various precipitation indices. This analysis aims to fill these gaps by delving into a comprehensive evaluation of the GSMaP Near-real-time Gauge-adjusted Rainfall Product version 6 (GSMaP-GNRT6) precipitation estimate over 20 years. Notably, China's complex terrain and diverse climate types, including the presence of the "Third Pole", the Tibetan Plateau, in western China, create challenges due to the combined impacts of the mid-latitude westerly wind and the East Asian monsoon [68–75]. Consequently, estimating precipitation based on satellite data remains a significant challenge due to the intricate spatial distribution and temporal evolution of precipitation in the region. This study aims to provide valuable references for both the application and enhancement of GSMaP-GNRT6 estimates.

The remainder of this analysis is structured as follows. Section 2 introduces the data and methods used in this study. The results are given in Section 3, including the verification of the GSMaP-GNRT6 data depicting the climatology, annual cycle, interannual variation and changing trends of accumulated precipitation, number of rainy days and rainstorm

days, and precipitation maxima in China from 2001 to 2020. A discussion about the main results of this analysis is presented in Section 4. The conclusions are presented in Section 5.

2. Data and Methods

In this analysis, the GSMaP-GNRT6 data were used [46]. These data are the gauge-adjusted precipitation levels, provided within four hours after observation and updated at one-hour intervals. Hourly precipitation is available in this dataset, while we adopted the daily product from 1 January 2001 to 31 December 2020. This dataset covers a domain of 50.05° – 239.95° E, 44.95° S– 39.95° N, with a horizontal resolution of $0.1^{\circ} \times 0.1^{\circ}$.

Using daily precipitation from 2419 national observation stations in China from 1 January 2001 to 31 December 2020, the GSMaP-GNRT6 data were verified by comparing China's precipitation climatology and climate variability. This dataset is compiled by the National Meteorological Information Center of the China Meteorological Administration, and primary quality control, such as spatiotemporal consistency checking and adjustment, is carried out. To meet the requirements of climate analysis, two additional steps were performed on the dataset. First, years in which the total number of missing records at a single station was greater than 20% were omitted. The second was to remove stations with continuous records of less than 15 years. Finally, 2378 stations were chosen for this analysis (Figure 1). The northern boundary of the GSMaP-GNRT6 data is at 39.95° N. To ensure a consistent spatial domain for comparison, the station data were interpolated into a $0.1^{\circ} \times 0.1^{\circ}$ grid in the domain of 72.05° – 123.95° E/ 18.05° – 39.95° N. And the Radial Basis Function (RBF) interpolation with a linear kernel was applied [76,77].

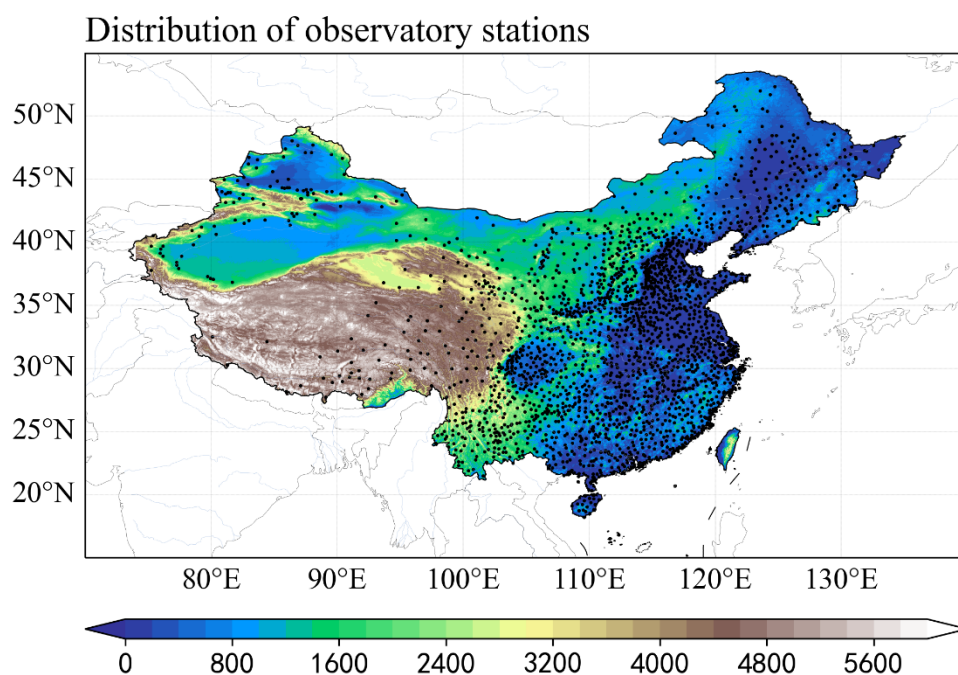


Figure 1. Distribution of observatory stations in China used in this analysis (black dots), shadings denoting the elevation of the terrain.

In this analysis, four precipitation indices were defined to validate the GSMaP-GNRT6 data, and their definitions are as follows:

Accumulated precipitation: the sum of precipitation in a period.

Rainy day: a day with daily precipitation equal to or greater than 0.1 mm [78].

Rainstorm day: a day with daily precipitation equal to or greater than 50 mm [79].

Precipitation maximum: the maximum precipitation in a period.

Based on the definitions, monthly and annual precipitation indices were analyzed in this study. The first two indices can represent the mean state of precipitation, while the

latter two indices are related to intense precipitation, reflecting the extreme characteristics of precipitation to a certain extent. By combining the mean state and extreme features, we conducted a comprehensive assessment of precipitation.

Meanwhile, the following four statistics were utilized to assess the performance of GSMaP-GNRT6 quantitatively:

$$\text{Absolute mean error (AME)} = \frac{1}{n} \sum_{i=1}^n |GSMaP_i - Observation_i|$$

$$\text{Relative error (RE)} = \frac{1}{n} \sum_{i=1}^n \left| \frac{GSMaP_i - Observation_i}{Observation_i} \right| * 100\%$$

$$\text{Root square mean error (RSME)} = \sqrt{\sum_{i=1}^n (GSMaP_i - Observation_i)^2 / n}$$

$$\text{Correlation coefficient} = \frac{\sum_{i=1}^n (GSMaP_i - \overline{GSMaP}) * (Observation_i - \overline{Observation})}{\sqrt{\sum_{i=1}^n (GSMaP_i - \overline{GSMaP})^2 / n} * \sqrt{\sum_{i=1}^n (Observation_i - \overline{Observation})^2 / n}}$$

where n is the sample size and \overline{GSMaP} and $\overline{Observation}$ represent the average of the GSMaP-GNRT6 data and station observations, respectively.

Climatology was averaged from 2001 to 2020. Statistical significance in correlation analysis was tested using the Student's t -test. Also, the linear trend coefficient was calculated by the least-squares method.

3. Results

First, we compare the spatial distribution and the annual cycle of mean precipitation, the number of rainy days, the number of rainstorm days and the precipitation maxima using GSMaP-GNRT6 data and station observations, respectively. This validation aims to evaluate the ability of GSMaP-GNRT6 to accurately represent the climatology of precipitation in China. Furthermore, given the abundance of precipitation in eastern China influenced by the East Asian subtropical rain belts, which makes the region susceptible to floods and droughts, we have dedicated a separate discussion to precipitation in eastern China. Additionally, the dense distribution of observation stations in eastern China, as shown in Figure 1, provides more reliable data for comparison with satellite-derived precipitation.

The annual precipitation pattern in China exhibits a decrease from the southeast to the northwest, with a peak of up to 1800 mm in the southeast and no more than 200 mm in the northwest (Figure 2a). The GSMaP-GNRT6 data capture this spatial distribution very well, and the precipitation amounts agree well with the station observations (Figure 2b). However, the GSMaP-GNRT6 data underestimate the annual precipitation amounts in the Yangtze River Valley, southern China and central-western China, while an overestimation is observed in the northern part of eastern China, the eastern and southern Tibetan Plateau (TP), and western Northwest China (Figure 2c). The AME ranges from 0 to 240 mm, and the high values above 240 mm are mainly located in the southern part of South China, eastern and central TP, and western Northwest China, indicating the large biases from station observations there (Figure 2d). Both the distribution and the magnitude of the RMSE are similar to those of the AME (Figure 2f). The RE of GSMaP-GNRT6 is below 20% in most areas of central and eastern China, while it ranges from 30% to 80% and even up to 90% in western Northwest China (Figure 2e). The distribution of RE shows a better performance of GSMaP-GNRT6 data in central and eastern China but a poorer representation in western China. However, it should be noted that the relatively low annual precipitation in western China may contribute to the large RE.

The ability of GSMaP-GNRT6 to depict the spatial pattern of monthly precipitation in China was assessed by spatial correlation analysis. As shown in Figure 3a, the spatial correlation coefficients for each month are consistently above 0.5, indicating that the GSMaP-GNRT6 data can well represent the spatial pattern of precipitation in China. And it can

be seen that the correlations in January, February and November are relatively lower, being around or below 0.6. In contrast, they are higher in the other months, peaking at 0.96 in May. In addition, GSMaP-GNRT6 shows a superior ability to represent the spatial distribution of precipitation in eastern China compared to the whole country, with all spatial correlations at 0.8 or above. In particular, the similarity between GSMaP-GNRT6 data and station observations is most pronounced from February to June, with spatial correlations exceeding 0.92 and reaching 0.96 in May and June. A comparison between China and eastern China indicates that the GSMaP-GNRT6-based precipitation in western China agrees less well with the station observations.

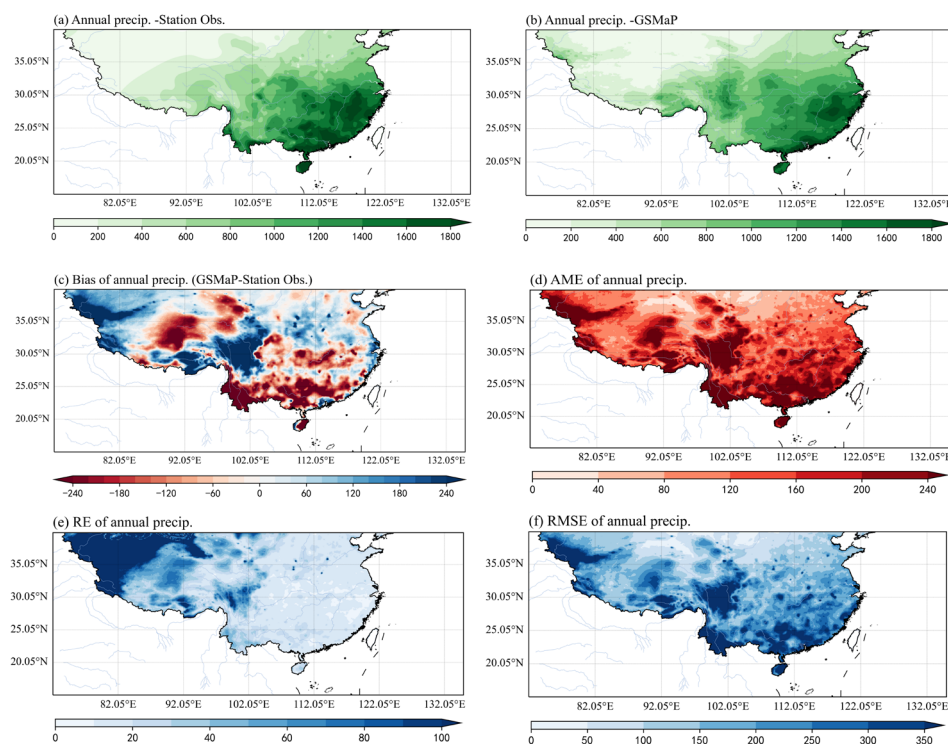


Figure 2. Distribution of annual precipitation in China based on station observations ((a), unit: mm) and GSMaP-GNRT6 data ((b), unit: mm), as well as biases ((c), unit: mm), absolute mean errors ((d), unit: mm), relative errors ((e), unit: %) and root mean square errors ((f), unit: mm) of GSMaP-GNRT6 data compared to station observations.

GSMaP-GNRT6 effectively depicts the seasonal cycle of precipitation in China, with the least precipitation in winter and the most precipitation in summer (Figure 4). Figure 4a shows that precipitation increases from January, peaks in July and gradually decreases until December. This development is consistent for both GSMaP-GNRT6 data and the station observations. However, the monthly precipitation of the GSMaP-GNRT6 data deviates from the station observations by 0.05 mm (March) to 32.5 mm (August), and the average deviation in China is 13.1 mm. Accordingly, the differences between GSMaP-GNRT6 data and station observations range from 0.12% (March) to 29.2% (November), with an average RE of 17.0%. In eastern China, the annual cycle of precipitation exhibits significant agreement between GSMaP-GNRT6 data and station observations (Figure 4b). The main difference is that the GSMaP-GNRT6 data indicate higher precipitation in the first half of the year compared to the station observations. Furthermore, the GSMaP-GNRT6 data show that the precipitation peak occurs in June, in contrast to the station observations in July. The AME of monthly precipitation in eastern China ranges from 0.45 mm (January) to 19.15 mm (June), and the mean AME is 7.11 mm. And the monthly GSMaP-GNRT6 precipitation deviates by 0.24% (October) to 33.40% (March) from the station observations, with an

average RE of 9.0%. Obviously, GSMaP-GNRT6 reflects the precipitation characteristics in eastern China more accurately than in western China.

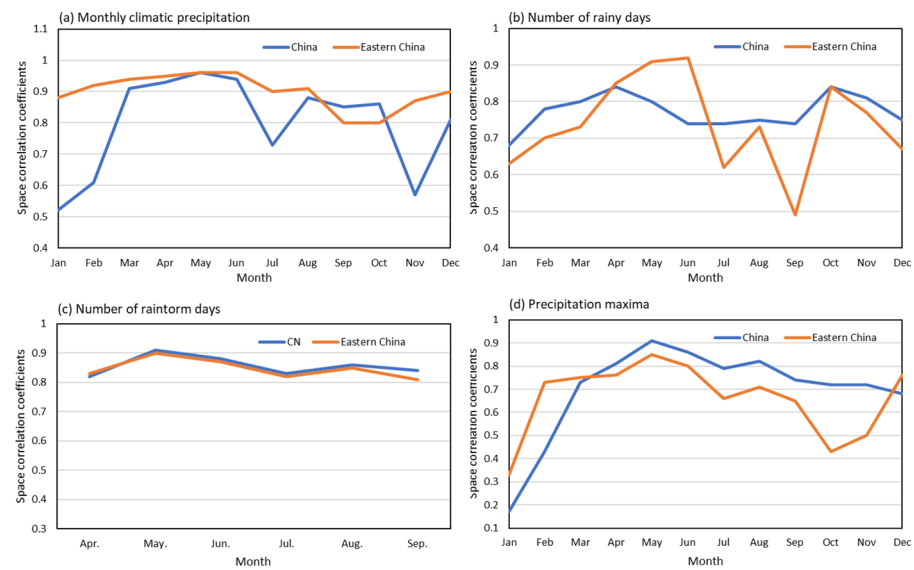


Figure 3. Spatial correlation coefficients of monthly climatic precipitation (a), number of rainy days (b), number of rainstorm days (c) and precipitation maxima (d) in China (blue lines, 72.05° – 122.55° E/ 17.55° – 39.95° N) and eastern China (orange lines, 105.05° – 122.55° E/ 17.55° – 39.95° N) between station observations and GSMaP-GNRT6 data.

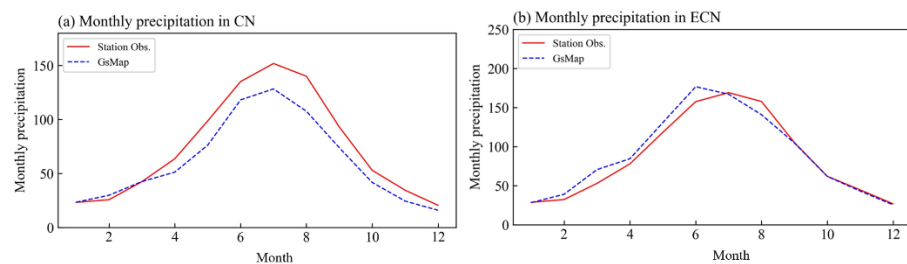


Figure 4. Climatological monthly precipitation averaged over China ((a), unit: mm) and eastern China ((b), unit: mm) based on station observations and GSMaP-GNRT6 data.

Similar to the spatial distribution of precipitation, the number of rainy days decreases from southeast to northwest (Figure 5a). GSMaP-GNRT6 captures this spatial pattern, but the belt with highest values is located in the north, along the Yangtze River Valley (Figure 5b). Due to this inconsistency in the high-value belt, the number of rainy days based on GSMaP-GNRT6 data is lower than that based on station observations in southern China and most of the TP, but higher in the eastern TP and north of the Yangtze River (Figure 5c). Additionally, the negative deviations are generally larger than the positive deviations. For both AME and RMSE, high values are found mainly in western South China and central TP, indicating a large error in these areas (Figure 5d,f). As shown in Figure 5e, the RE of GSMaP-GNRT6 data is generally less than 20% in most areas of central and eastern China but is larger in western South China, western TP and western Northwest China. Additionally, a large error is observed at the northwestern edge of the TP.

The monthly spatial correlation of the number of rainy days in China between GSMaP-GNRT6 data and station observations is stable at or above 0.7, peaking at 0.84 in April and October (Figure 3b). These high correlation coefficients confirm that GSMaP-GNRT6 reflects the spatial distribution of the number of rainy days in China well. At the same time, it should be noted that the ability of GSMaP-GNRT6 to depict the spatial pattern of the number of rainy days in eastern China varies depending on the month. The correlation

coefficients are generally higher in the first half of the year, exceeding 0.9 in May and June, but dropping to less than 0.5 in September.

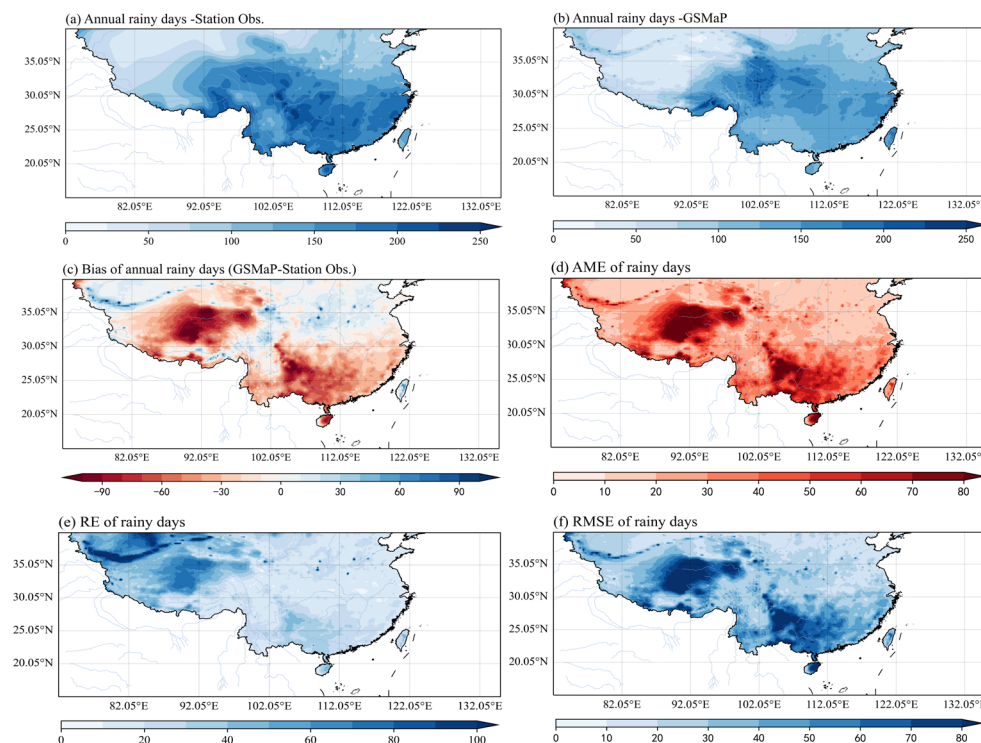


Figure 5. Distribution of the annual number of rainy days in China based on station observations ((a), unit: days) and GSMaP-GNRT6 data ((b), unit: days), as well as biases ((c), unit: days), absolute mean errors ((d), unit: days), relative errors ((e), unit: %) and root mean square errors ((f), unit: days) of GSMaP-GNRT6 data compared to station observations.

GSMaP-GNRT6 records the annual cycle of an increase in the first half of the year and a decrease in the second half of the year in terms of the number of rainy days in China, with the peak in July (Figure 6). Nevertheless, the number of rainy days derived from GSMaP-GNRT6 data is lower by 1.36 days (July) to 3.96 days (January) and by 8.5% (July) to 50.2% (December) compared to station observations in each month. The mean AME and RE are 2.37 days and 24.9%, respectively. This consistent underestimation of the number of rainy days indicates a general underestimation of precipitation. In eastern China, the underestimation by GSMaP-GNRT6 is much smaller and occurs mainly in the winter months. The AME ranges from 0.05 days (May) to 3.85 days (January), with an average of 1.3 days. And the RE is 0.34% (May) to 41.3% (March), with an average of 13.0% (Figure 6b).

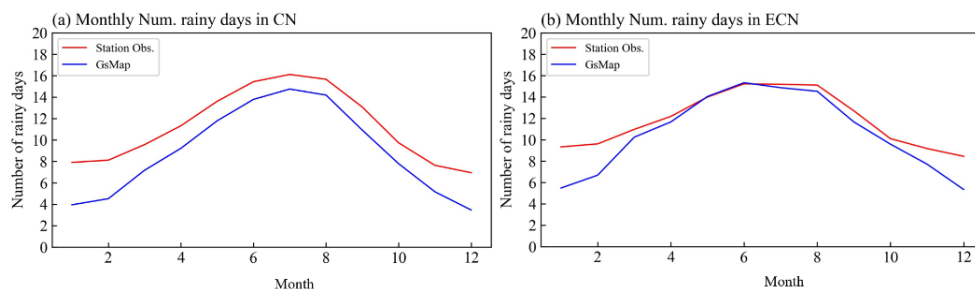


Figure 6. Climatological monthly number of rainy days averaged over China ((a), unit: days) and eastern China ((b), unit: days) based on station observations and GSMaP-GNRT6 data.

As heavy rainfall mainly occurs in summer, the number of rainstorm days is analyzed from April to September. Rainstorms are concentrated in southeastern China, especially in the southern coastal areas, where the maximum annual number of rainstorm days reaches about 10 days (Figure 7a). In contrast, they rarely occur in northern and western China. The GSMaP-GNRT6 data reflect the spatial pattern well (Figure 7b). However, the number of rainstorm days is underestimated in most of eastern China, while it is slightly overestimated in western China by the GSMaP-GNRT6 data, resulting in a pattern of “less in eastern China but more in western China” compared to the station observations (Figure 7c). High values for AME and RMSE are mainly observed in the southeastern part of China, where rainstorms occur frequently (Figure 7d,f). In this region, the RE of GSMaP-GNRT6 is between 20% and 50% in most parts but is much higher in the northern and western fringes (Figure 7e).

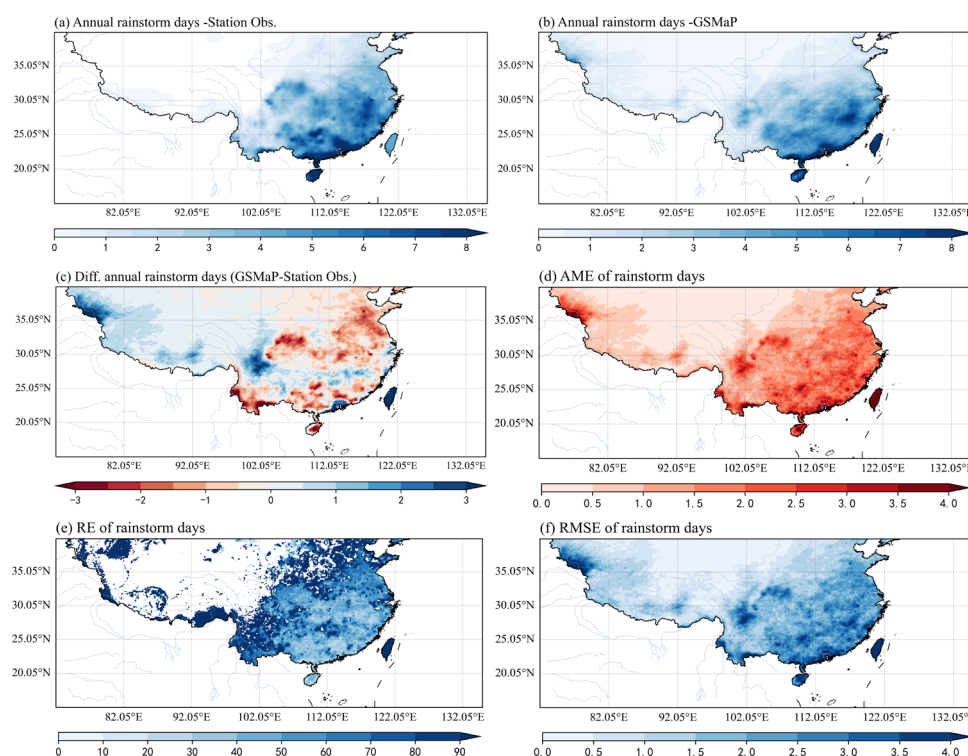


Figure 7. Distribution of the annual number of rainstorm days in China based on station observations ((a), unit: days) and GSMaP-GNRT6 data ((b), unit: days), as well as biases ((c), unit: days), absolute mean errors ((d), unit: days), relative errors ((e), empty areas indicating no occurrence of rainstorm by station observations, unit: %) and root mean square errors ((f), unit: days) of GSMaP-GNRT6 data relative to station observations.

The monthly spatial correlations in the number of rainstorm days between the GSMaP-GNRT6 data and the station observations are consistently higher than 0.8, reaching 0.9 in May for both China and eastern China (Figure 3c). This high degree of agreement indicates that GSMaP-GNRT6 represents the spatial patterns of heavy precipitation well.

Rainstorms are rare in the winter months, gradually increasing from spring to summer and then decreasing again (Figure 8). Both the GSMaP-GNRT6 data and the station observations capture this annual cycle. In addition, the GSMaP-GNRT6 data underestimate the number of rainstorm days from April to September by 0.05 days (September) to 0.26 days (July), with an average of 0.15 days in China. Accordingly, the number of rainstorm days derived from the GSMaP-GNRT6 data is between 26.1% (May) and 52.4% (July), and thus on average 39.5% below the station observations. The situation is similar in eastern China, where the number of rainstorm days is underestimated by GSMaP-GNRT6 data by 0.02 days (May) to 0.27 days (July) and 3.0% (May) to 39.8% (July), with average values

of 0.11 day and 21.7%, respectively. Better performance in representing the occurrence of rainstorm days by GSMaP-GNRT6 data is also observed in eastern China. In addition, the peak of the number of rainstorm days in GSMaP-GNRT6 occurs earlier, in May, compared to June in the station observations.

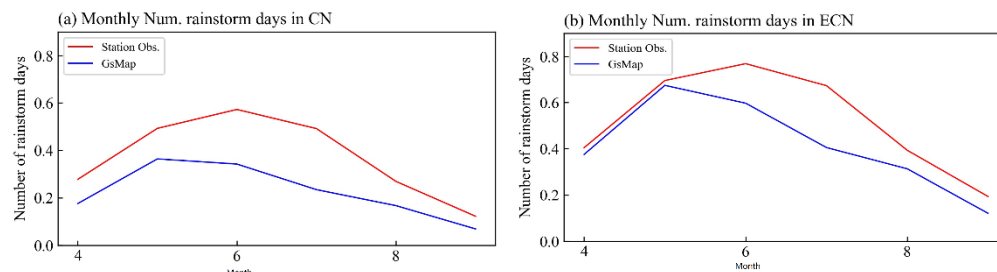


Figure 8. Climatological monthly number of rainstorm days averaged over China ((a), unit: days) and eastern China ((b), unit: days) based on station observations and GSMaP-GNRT6 data.

The comparison of daily precipitation maxima is made to assess the ability of GSMaP-GNRT6 to depict extreme precipitation. Climatologically, the daily precipitation maxima in eastern and southern China exceed almost 80 mm (Figure 9a). The scattered distribution of high values illustrates the localized nature of precipitation, which is influenced by factors such as terrain elevation and small- to medium-scale weather systems. The GSMaP-GNRT6 data demonstrate a similar spatial pattern of daily maximum precipitation in China (Figure 9b). The differences in precipitation maxima between GSMaP-GNRT6 and the station observations show a pattern of negative biases in parts of eastern China and positive biases in western China (Figure 9c). This pattern indicates an underestimation in the east and an overestimation in the west by GSMaP-GNRT6, similar to the number of rainstorm days. The AME and RMSE are consistently greater than 20 mm/day in most parts of China, with the higher values in southeastern China and the western part of western China (Figure 9d,f). Seen from Figure 9e, GSMaP-GNRT6 overestimates the number of rainstorm days by 20% to 30% in eastern China, while it underestimates it by more than 60% in western China.

As far as the monthly precipitation maxima in China are concerned, the spatial distribution in January is very different, with a spatial correlation of less than 0.2 (Figure 3d). In the other months, however, the precipitation maxima from GSMaP-GNRT6 show a very similar spatial pattern to those from the station observations, with spatial correlations consistently around or above 0.7, peaking at over 0.9 in May. The situation in eastern China is similar.

For both China and eastern China, there are obvious differences in the annual cycle of precipitation maxima presented by GSMaP-GNRT6 data and station observations (Figure 10). The station observations show an increase from January to July, followed by a decrease. In contrast, the GSMaP-GNRT6 data exhibit a much more even variation. The precipitation maxima in GSMaP-GNRT6 are larger at the beginning and end of the year than in the station observations, but the opposite is true in the middle of the year. The AME between the two datasets ranges from 1.36 mm (April) to 44.0 mm (February) in China, with an average of 23.9 mm. And the RE varies from 2.5% (April) to 163.0% (February), and the average is 49.1%. In eastern China, the AME of GSMaP-GNRT6 ranges from 2.1 mm (November) to 39.7 mm (July) and from 3.5% (November) to 102.8% (January). The average AME and RE are 21.3 mm and 36.6%, respectively.

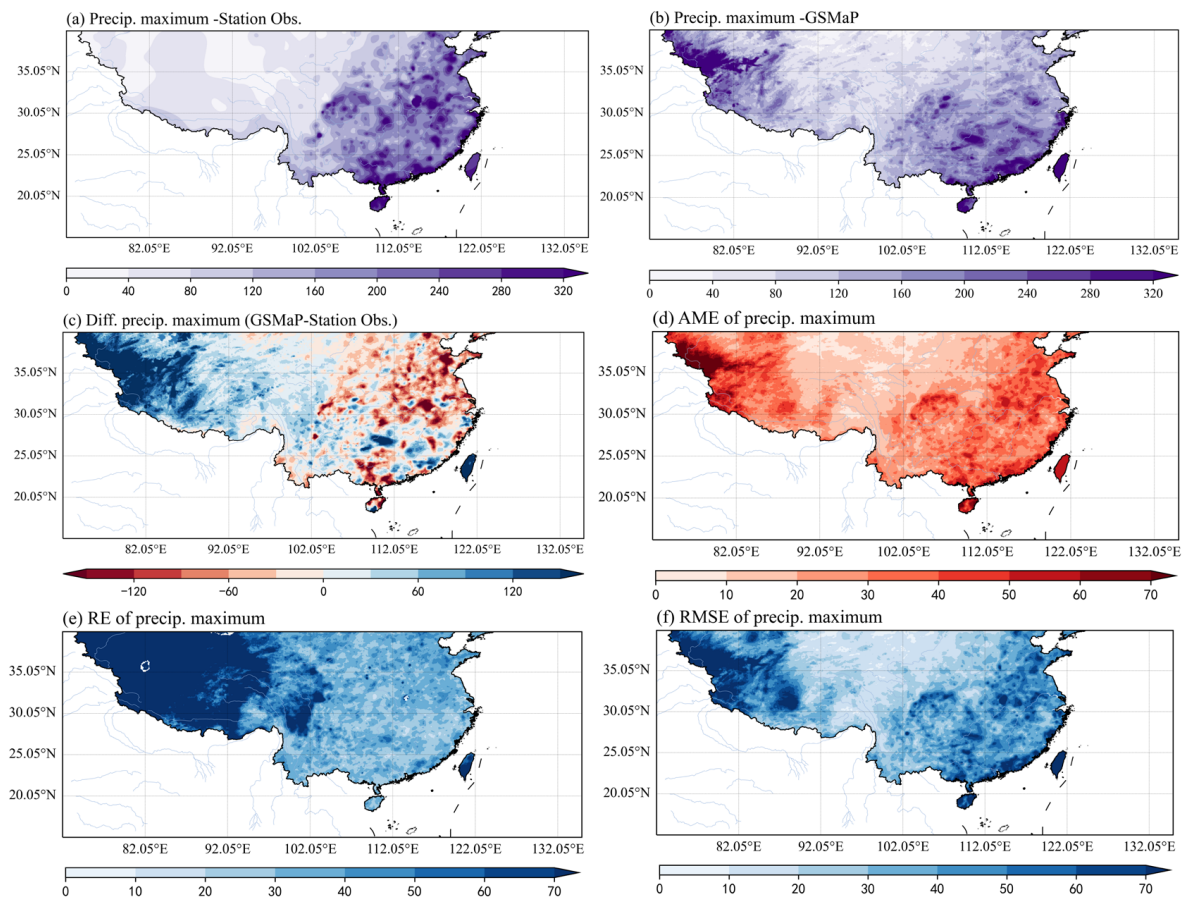


Figure 9. Distribution of the annual precipitation maxima in China based on station observations ((a), unit: mm) and GSMaP-GNRT6 data ((b), unit: mm), as well as biases ((c), unit: mm), absolute mean errors ((d), unit: mm), relative errors ((e), unit: %) and root mean square errors ((f), unit: mm) of GSMaP-GNRT6 data compared to station observations.

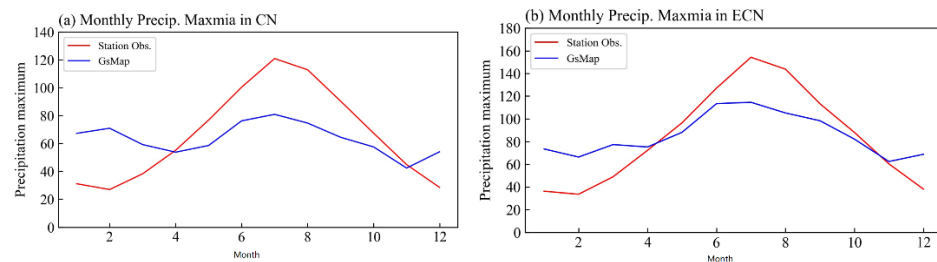


Figure 10. Climatological monthly precipitation maxima averaged over China ((a), unit: mm) and eastern China ((b), unit: mm) based on station observations and GSMaP-GNRT6 data.

Considering the potential of the GSMaP-GNRT6 data with 20-year records for exploring and understanding climate variability, we performed a validation focusing on the interannual variation and changing trends using the four precipitation indices. The correlation coefficients of annual precipitation between the GSMaP-GNRT6 data and the station observations from 2001 to 2020 were calculated for each grid and the distributions are shown in Figure 11. It is obvious that the annual precipitation has the highest correlation, especially in central and eastern China, which reaches up to 0.537 and exceeds the confidence level of 0.99 (Figure 11a). In western China, on the other hand, the correlation between the two datasets is weak. GSMaP-GNRT6 only captures the interannual variation in the number of rainy days to a limited extent (Figure 11b). Correlation coefficients greater than 0.423 and exceeding the 95% confidence level are only observed in some

parts of southeastern China and the TP. GSMaP-GNRT6 depicts the interannual variation in the number of rainstorm days in most eastern regions of China and northern–central China well but shows an opposite variation to the station observations in western China (Figure 11c). The correlation of the precipitation maxima shows a clear discrete spatial distribution (Figure 11d). However, high positive correlation coefficients dominate in eastern China, indicating a coherence of the interannual variation between GSMaP-GNRT6 data and station observations.

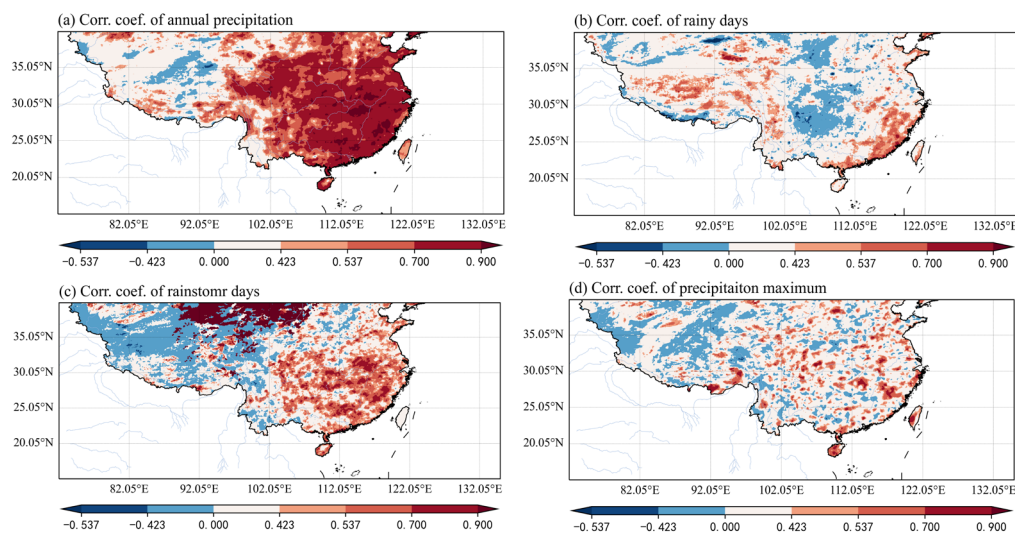


Figure 11. Distribution of correlation coefficients of annual precipitation (a), number of rainy days (b), number of rainstorm days (c) and precipitation maxima (d) across China from 2001 to 2020 between station observations and GSMaP-GNRT6 data.

The correlation coefficients between the GSMaP-GNRT6 data and the station observations were also calculated for the precipitation indices averaged over China and eastern China. As shown in Figure 12a,e, the annual precipitation and the number of rainstorm days in China show a coherent interannual variation, with the correlation coefficients both being up to 0.76, exceeding the 99.9% confidence level. The correlation of the precipitation maxima in China between the two datasets is 0.46, exceeding the confidence level of 95%. However, the inconsistencies become clearer after the early 2010s (Figure 12g). The temporal variation in the number of rainy days in China is less consistent between the two datasets, with a correlation of only -0.16 (Figure 12c). It is noteworthy that all four precipitation indices show an obvious underestimation of GSMaP-GNRT6 in China, with the average AME and RE being 155.8 mm and 17.6% for annual precipitation, 35.5 days and 24.1% for the number of rainy days, 0.8 days and 31.6% for the number of rainstorm days, and 8.5 mm and 11.8% for precipitation maxima, respectively. This observation aligns with the findings in the climatological comparisons. In eastern China, GSMaP-GNRT6 data and station observations demonstrate highly coherent interannual variation in annual precipitation, the number of rainstorm days and precipitation maxima, with correlations of 0.83, 0.80 and 0.66, respectively, exceeding the confidence level of 99%. However, the opposite variation in the number of rainy days between the two datasets is significant (Figure 12d). And it is evident that the differences in the magnitude of precipitation indices between the two datasets is reduced significantly. The average AME and RE is 58.4 mm and 5.5% for annual precipitation, 21.9 days and 24.1% for the number of rainy days, 0.5 day and 15.4% for the number of rainstorm days, and 5.0 mm and 6.0% for precipitation maxima, respectively. In particular, the annual precipitation based on the two datasets is almost identical before the early 2010s. By comparison, in interannual variation, the underestimation of GSMaP-GNRT6 and better depiction in eastern China are proved again.

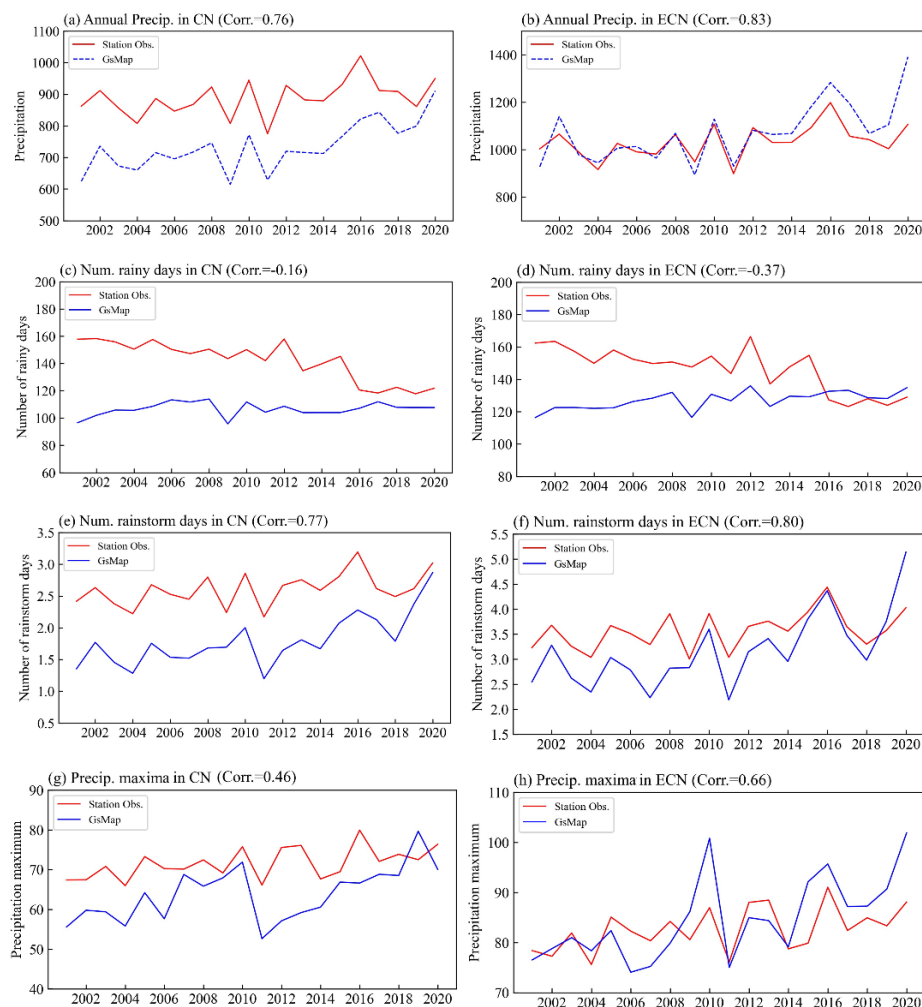


Figure 12. Time series of annual precipitation ((a,b), unit: mm), number of rainy days ((c,d), unit: days), number of rainstorm days ((e,f), unit: days) and precipitation maxima ((g,h), unit: mm) across China (a,c,e,g) and eastern China (b,d,f,h) from 2001 to 2020 based on station observations and GsMaP-GNRT6 data.

Figure 13 presents the monthly correlations of temporal evolution for each precipitation index between GsMaP-GNRT6 data and station observations. It is evident that the consistency of annual precipitation between the two datasets is the highest, with correlations all above 0.6 and reaching 0.92 (Figure 13a). Moreover, the temporal variation in annual precipitation is more coherent in eastern China than in the whole of China. GsMaP-GNRT6 data also well depict the interannual variation in number of rainstorm days and precipitation maxima, with higher consistency in eastern China, where the correlation coefficients are generally higher (Figure 13c,d). The minimum correlation is above 0.4, while the maximum correlation reaches 0.91. It can also be observed that the coherence of interannual variation between the two datasets is higher in the latter half of the year. GsMaP-GNRT6 does not depict the interannual variation in the monthly number of rainy days well (Figure 13b). Its correlations with station observations in June and July are notably lower and even opposite for China, with the maximum correlation being only 0.52 in October. The situation improves in eastern China, especially in the latter half of the year, when the correlations are consistently above 0.6.

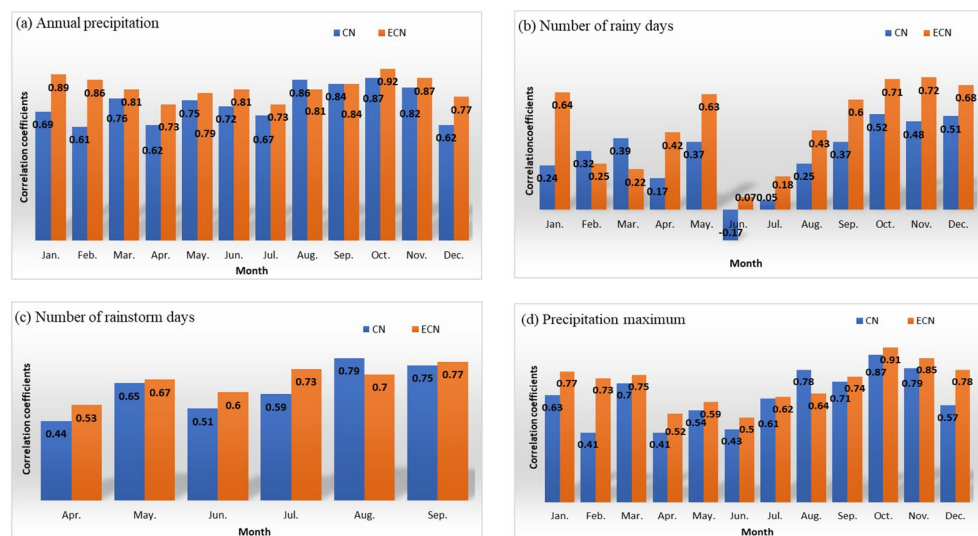


Figure 13. Correlation coefficients of monthly precipitation ((a), unit: mm), number of rainy days ((b), unit: days), number of rainstorm days ((c), unit: days) and precipitation maxima ((d), unit: mm) averaged over China and eastern China between station observations and GSMaP-GNRT6 data.

In addition to interannual variation, changing trends in four precipitation indices based on GSMaP-GNRT6 were also assessed. Comparing Figure 14a with Figure 14b, increasing trends of annual precipitation in most of China are coherent between GSMaP-GNRT6 data and station observations, with high and positive values located in southern China. However, both the extent and magnitude of increase rates are greater in the GSMaP-GNRT6 data compared to the station observations. The regions with an annual precipitation increase rate greater than 150 mm/decade cover most of southern China according to GSMaP-GNRT6 data, while they are only located in the lower reaches of the Yangtze River Valley and some parts of eastern Southwest China according to station observations. Changes in the number of rainy days derived by GSMaP-GNRT6 present an “increase in the east but a decrease in the west” pattern (Figure 14c). And the upward trend along the middle and lower reaches of the Yangtze River Valley and the downward trend in the central Tibetan Plateau exceed the confidence level of 95%, with the changing rate over ± 10 days/decade. However, the situation is different from the significant decreasing trend in the whole of China derived from station observations, with a rate lower than -16 days/decade (Figure 14d). Increasing trends dominate the changes in the number of rainstorm days and annual precipitation maxima (Figure 14e–h). Both GSMaP-GNRT6 data and station observations capture this feature, while some discrepancy is observed in the extent and magnitude of increasing trends. Obviously, GSMaP-GNRT6 data tend to show a larger increasing trend in all four precipitation indices than station observations. We also compared the changing trends in four precipitation indices averaged over China and eastern China between the two datasets, and similar results were obtained. Moreover, it was found that GSMaP-GNRT6 shows an accelerated growth trend after the early 2010s, and the difference from station observations expands.

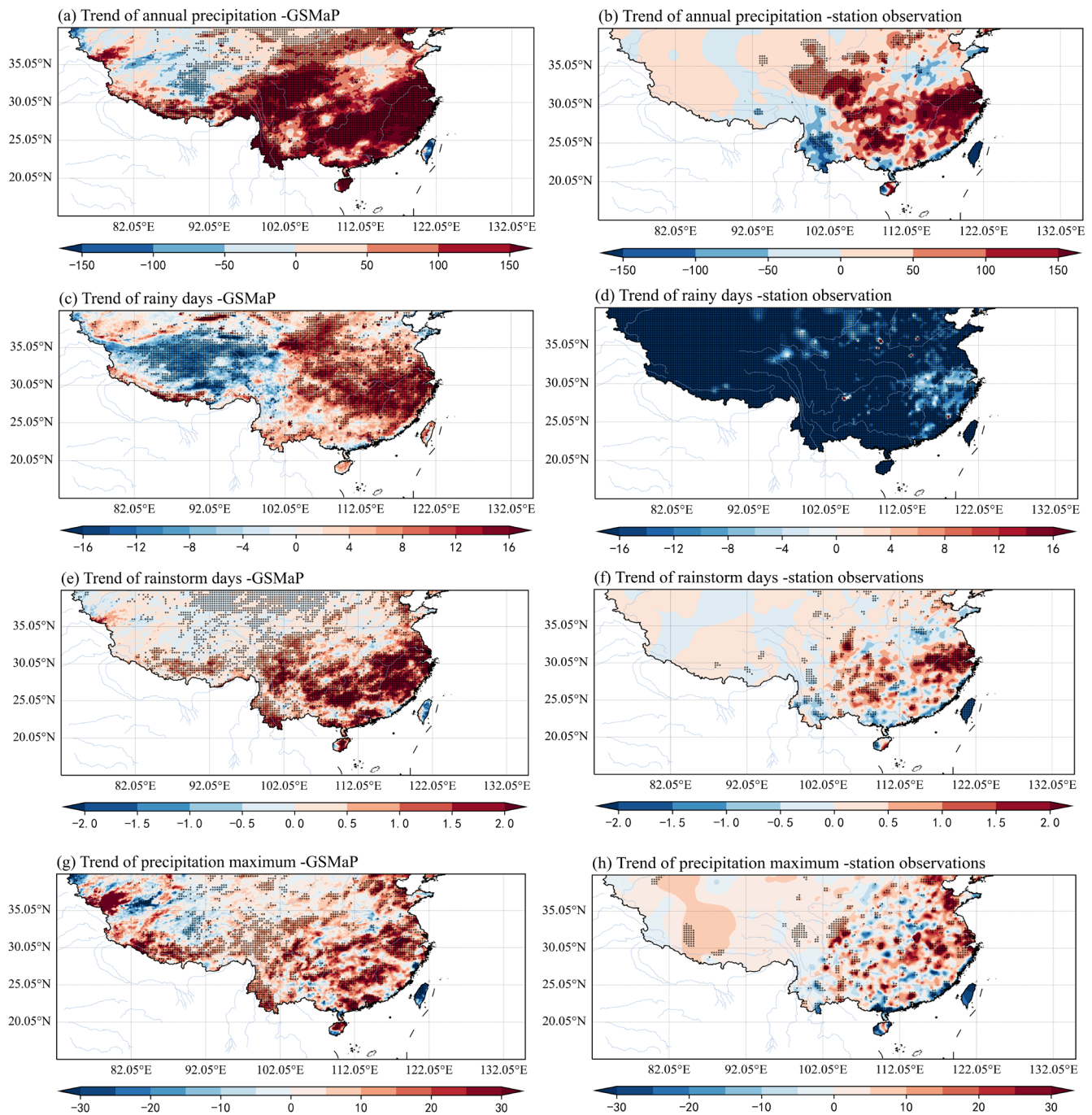


Figure 14. Linear trend coefficients of annual precipitation ((a,b), unit: mm/decade), number of rainy days ((c,d), unit: days/decade), number of rainstorm days ((e,f), unit: days/decade) and precipitation maxima ((g,h), unit: mm/decade) in China based on GSMaP-GNRT6 data (a,c,e,g) and station observations (b,d,f,h), with the black dots indicating exceeding the confidence level of 95%.

4. Discussions

The reliability of GSMaP data in presenting the spatial distribution and temporal variation in precipitation in China has previously been validated by numerous studies [61–64]. In this analysis, this consistency is further affirmed through long-term records and extensive station observations for comparison. Moreover, unlike previous studies that only focused on rainfall amounts, this analysis also looked at the number of rainy days and rainstorm days and precipitation maxima. By these indices, both climate states and extremes in precipitation were investigated. In addition, different

time scales, such as annual cycles, interannual variations and changing trends, were further discussed in this analysis. Therefore, more information is provided for reference GSMaP-GNRT6 data applications and improvements. However, it is important to acknowledge the uncertainties. Firstly, the spatial distribution of observatory stations is uneven, with a high density in eastern China but with stations scattered in the western region (Figure 1). This disparity can impact on the comparison results to some extent. Additionally, station observations provide local precipitation data in situ, whereas the GSMaP-GNRT6 data represent precipitation in a $0.1^\circ \times 0.1^\circ$ grid. This difference in spatial representation introduces uncertainties in validation results [53,80–83]. Furthermore, undetected errors in station records, interpolation methods and other factors can also contribute to uncertainties. It is crucial to recognize these uncertainties and associated limitations. In addition, as the GSMaP-GNRT6 data used in this analysis were limited to the region south of 39.95°N , a comparison of precipitation in Northeast China and Northwest China was absent from this study. As a result, the obtained conclusions have some limitations related to spatial coverage. It is essential to perform a supplementary analysis encompassing the entirety of China once the GSMaP-GNRT6 data for the northern region above 39.95°N become available.

In this analysis, a notable overestimate was observed over the Tibetan Plateau for all four precipitation indices. Due to the unique terrain and the absence of reference data from station observations, estimating precipitation on the Tibetan Plateau is a challenge and involves certain uncertainties [84–86]. The same challenges are encountered in other mountainous and plateau areas.

A greater increasing trend was observed in the number of rainy days based on GSMaP-GNRT6 data compared to the station observations. However, many previous studies have highlighted a decrease in rainy days but an increase in precipitation intensity in China [87–89]. The biases in light rainfall estimates by the GSMaP data may contribute to this discrepancy [61,90,91]. Therefore, there is room for improvement in the GSMaP's ability to identify whether precipitation occurs and estimate precipitation of different intensities. Retrieval algorithms, the number of passive microwave samples, sensor capabilities, spatiotemporal resolution and coverage area constitute the primary sources of error in satellite-derived precipitation data [92]. Consequently, advancements in retrieval algorithms, enhancements in observation instruments and technologies, an increase in passive microwave samples, and improvements in resolution are key factors in enhancing the reliability of satellite precipitation estimates [93]. Simultaneously, various correction methods have been developed to improve their reliability. Notably, the adjustment of daily gauge data plays a crucial role in refining GSMaP estimates [83,93]. Polynomial fitting has been proven to be effective [94], and geographically weighted regression contributes to error reduction and facilitates the attainment of higher-spatial-resolution data [95].

GSMaP-GNRT6 data can be applied to climate change research, but caution is advised regarding the overestimation of increasing trends in precipitation indices, especially concerning the number of rainy days. And efforts should be taken to investigate the potential causes of the excessive increase observed after the early 21st century.

5. Conclusions

The GSMaP data provide global precipitation estimates with high spatial and temporal resolution. In order to better apply this dataset and facilitate its development, this study conducted a comprehensive validation of the GSMaP-GNRT6 data using four precipitation indices, including accumulated precipitation, number of rainy days, number of rainstorm days and precipitation maxima, by comparing them with observation data from 2419 stations in China, based on 20-year records from 2001 to 2020.

The GSMaP-GNRT6 data generally well capture the spatial distribution of the four precipitation indices in China. The spatial correlations between the GSMaP-GNRT6 data and station observations are above 0.7 in most months, particularly for the number of rainstorm days, where the spatial correlations exceed 0.8 in each month over both China and eastern

China. GSMaP-GNRT6 depicts the spatial distribution of annual precipitation averaged over eastern China better than that over China. Conversely, for the other three indices, the GSMaP-GNRT6 data perform better in accurately depicting the spatial distribution over the entire country. However, GSMaP-GNRT6 shows some limitations in accurately depicting the spatial distribution of the number of rainy days from July to September and precipitation maxima during wintertime over eastern China.

A general underestimation of the GSMaP-GNRT6 data was observed. The monthly precipitation is underestimated by 17.0% by the GSMaP-GNRT6 in China on average, and the monthly number of rainy days and rainstorm days, as well as the monthly precipitation maxima, are underestimated by 24.9%, 39.5% and 49.1%, respectively. Compared with station observations, the annual precipitation, number of rainy days and rainstorm days, and precipitation maxima based on the GSMaP-GNRT6 data are 17.6%, 35.5%, 31.6% and 11.8% less, respectively. GSMaP-GNRT6 depicts precipitation in eastern China better, with the errors almost halved. However, the number of rainstorm days and maximum precipitation are significantly overestimated, even by more than 60%.

The GSMaP-GNRT6 data effectively capture the annual cycle of all four precipitation indices, but the annual cycle in precipitation maxima based on the GSMaP-GNRT6 data is much smoother compared to station observations. The GSMaP-GNRT6 demonstrates a strong ability to represent the interannual variation in accumulated precipitation, the number of rainstorm days and precipitation maxima, particularly for the former two indices, where the correlation coefficients with station observations exceed 0.75. However, a noticeable discrepancy in the interannual variation in the number of rainy days is evident. Similarly, accumulated precipitation, the number of rainstorm days and precipitation maxima based on the GSMaP-GNRT6 data exhibit a consistent increasing trend comparable to that observed by station observations. Nevertheless, the GSMaP-GNRT6 data tend to overestimate this upward trend, especially entering the early 21st century. Regarding the number of rainy days in China, an opposite changing trend was observed between the GSMaP-GNRT6 data and station observations, with an upward trend in the former and a downward trend in the latter.

Author Contributions: Conceptualization, Z.W.; methodology, Z.W.; formal analysis, Z.W.; investigation, Q.L.; resources, Z.W.; data curation, Z.W.; writing—original draft preparation, Z.W.; writing—review and editing, Z.W. and Q.L.; visualization, Z.W.; supervision, Z.W.; project administration, Q.L.; funding acquisition, Q.L. All authors have read and agreed to the published version of the manuscript.

Funding: This research is supported by the National Key Research and Development Program of China (2022YFE0136000) and the National Natural Science Foundation of China (U2242207).

Data Availability Statement: The data from 2419 meteorological stations in China are available from the National Meteorological Information Center of the China Meteorological Administration at <http://data.cma.cn/> (accessed on 1 February 2022). The GSMaP-GNRT6-GNRT6 data are provided by the Japan Aerospace Exploration Agency (JAXA) (<https://earth.jaxa.jp/en/data/index.html> (accessed on 1 March 2023)).

Acknowledgments: We acknowledge the World Meteorological Organization for initiating the Space-Based Weather and Climate Extremes Monitoring (SWCEM) project and triggering this analysis. We are grateful to Takuji Kubota of the Japan Aerospace Exploration Agency (JAXA) for providing the data. We would also like to thank Yuri Kuleshov from the National Climate Center, the Australian Bureau of Meteorology, for his invaluable recommendations and unwavering support.

Conflicts of Interest: The authors declare no conflicts of interest.

References

1. Schär, C.; Frei, C. Orographic precipitation and climate change. *Glob. Change Mt. Reg. Overv. Curr. Knowl.* **2005**, *23*, 255–266.
2. Douben, K.J. Characteristics of river floods and flooding: A global overview, 1985–2003. *Irrig. Drain.* **2006**, *55*, S9–S21. [CrossRef]
3. Petley, D. Global patterns of loss of life from landslides. *Geology* **2012**, *40*, 927–957. [CrossRef]

4. Hirabayashi, Y.; Mahendran, R.; Koirala, S.; Konoshima, L.; Yamazaki, D.; Watanabe, S.; Kim, H.; Kanae, S. Global flood risk under climate change. *Nat. Clim. Chang.* **2013**, *3*, 816–821. [[CrossRef](#)]
5. Dowling, C.A.; Santi, P.M. Debris flows and their toll on human life: A global analysis of debris-flow fatalities from 1950 to 2011. *Nat. Hazards* **2014**, *71*, 203–227. [[CrossRef](#)]
6. Yang, T.H.; Gong, D.H.; Chin, C.T.; Jui, Y.H. Using rainfall thresholds and ensemble precipitation forecasts to issue and improve urban inundation alerts. *Hydrol. Earth Syst. Sci.* **2016**, *20*, 4731. [[CrossRef](#)]
7. Li, X.; Rankin, C.; Gangrade, S.; Zhao, G.; Lander, K.; Voisin, N.; Shao, M.; Morales-Hernández, M.; Kao, S.C.; Gao, H. Evaluating precipitation, streamflow, and inundation forecasting skills during extreme weather events: A case study for an urban watershed. *J. Hydrol.* **2021**, *603*, 127126. [[CrossRef](#)]
8. Trenberth, K.E. The impact of climate change and variability on heavy precipitation, floods, and droughts. In *Encyclopedia of Hydrological Sciences*; John Wiley & Sons, Ltd.: Hoboken, NJ, USA, 2005; Volume 17, pp. 1–11.
9. Dai, A. Drought under global warming: A review. *Wiley Interdiscip. Rev. Clim. Chang.* **2011**, *2*, 45–65. [[CrossRef](#)]
10. Mukherjee, S.; Mishra, A.; Trenberth, K.E. Climate change and drought: A perspective on drought indices. *Curr. Clim. Chang. Rep.* **2018**, *4*, 145–163. [[CrossRef](#)]
11. Dai, A.; Zhao, T.; Chen, J. Climate Change and Drought: A Precipitation and Evaporation Perspective. *Curr. Clim. Chang.* **2018**, 301–312. [[CrossRef](#)]
12. Wang, Z.; Zhang, Q.; Sun, S.; Wang, P. Interdecadal variation of the number of days with drought in China based on the standardized precipitation evapotranspiration index (SPEI). *J. Clim.* **2022**, *35*, 2003–2018. [[CrossRef](#)]
13. Tebaldi, C.; Hayhoe, K.; Arblaster, J.M.; Meehl, G.A. Going to the extremes. *Clim. Chang.* **2006**, *79*, 185–211. [[CrossRef](#)]
14. Schmidt, S.; Kemfert, C.; Höpfe, P. The impact of socio-economics and climate change on tropical cyclone losses in the USA. *Reg. Environ. Chang.* **2010**, *10*, 13–26. [[CrossRef](#)]
15. Stocker, T.; Qin, D.; Plattner, G.; Tignor, M.; Allen, S.; Boschung, J.; Nauels, A.; Xia, Y.; Bex, V.; Midgley, P. *Climate Change 2013: The Physical Science Basis: Working Group I Contribution to the Fifth Assessment Report of the Intergovernmental Panel on Climate Change*; Cambridge University Press: Cambridge, UK, 2013; pp. 167–178.
16. Mullan, D.; Favis-Mortlock, D.; Fealy, R. Addressing key limitations associated with modelling soil erosion under the impacts of future climate change. *Agric. For. Meteorol.* **2012**, *156*, 18–30. [[CrossRef](#)]
17. Woodward, G.; Bonada, N.; Brown, L.E.; Death, R.G.; Durance, I.; Gray, C.; Hladyz, S.; Ledger, M.E.; Milner, A.M.; Ormerod, S.J. The effects of climatic fluctuations and extreme events on running water ecosystems. *Philos. Trans. R. Soc. B* **2016**, *371*, 20150274. [[CrossRef](#)] [[PubMed](#)]
18. Paerl, H.W.; Crosswell, J.R.; Van, D.B.; Hall, N.S.; Rossignol, K.L.; Osburn, C.L.; Hounshell, A.G.; Sloup, R.S.; Harding, L.W. Two decades of tropical cyclone impacts on North Carolina’s estuarine carbon, nutrient and phytoplankton dynamics: Implications for biogeochemical cycling and water quality in a stormier world. *Biogeochemistry* **2018**, *141*, 307–332. [[CrossRef](#)]
19. Allen, M.R.; Ingram, W.J. Constraints on future changes in climate and the hydrologic cycle. *Nature* **2002**, *419*, 228–232. [[CrossRef](#)]
20. Santer, B.D.; Mears, C.; Wentz, F.; Taylor, K.; Gleckler, P.; Wigley, T.; Barnett, T.; Boyle, J.; Brüggemann, W.; Gillett, N. Identification of human-induced changes in atmospheric moisture content. *Proc. Natl. Acad. Sci. USA* **2007**, *104*, 15248–15253. [[CrossRef](#)]
21. Min, S.K.; Zhang, X.; Zwiers, F.W.; Hegerl, G.C. Human contribution to more-intense precipitation extremes. *Nature* **2011**, *470*, 378–381. [[CrossRef](#)]
22. Roderick, T.P.; Wasko, C.; Sharma, A. Atmospheric moisture measurements explain increases in tropical rainfall extremes. *Geophys. Res. Lett.* **2019**, *46*, 1375–1382. [[CrossRef](#)]
23. Tan, X.; Wu, X.; Liu, B. Global changes in the spatial extents of precipitation extremes. *Environ. Res. Lett.* **2021**, *16*, 054017. [[CrossRef](#)]
24. Arkin, P.A.; Ardanuy, P.E. Estimating climatic-scale precipitation from space: A review. *J. Clim.* **1989**, *2*, 1229–1238. [[CrossRef](#)]
25. Trenberth, K.E.; Dai, A.; Rasmussen, R.M.; Parsons, D.B. The Changing Character of Precipitation. *Bull. Am. Meteorol. Soc.* **2003**, *84*, 1205–1217. [[CrossRef](#)]
26. Daly, C.; Halbleib, M.; Smith, J.I.; Gibson, W.P.; Doggett, M.K.; Taylor, G.H.; Curtis, J.; Pasteris, P.P. Physiographically sensitive mapping of climatological temperature and precipitation across the conterminous United States. *Int. J. Climatol.* **2008**, *28*, 2031–2064. [[CrossRef](#)]
27. Michaelides, S.; Levizzani, V.; Anagnostou, E.; Bauer, P.; Kasparis, T.; Lane, J.E. Precipitation: Measurement, remote sensing, climatology and modeling. *Atmos. Res.* **2009**, *94*, 512–533. [[CrossRef](#)]
28. Stephens, G.L.; L’Ecuyer, T.; Forbes, R.; Gettelmen, A.; Golaz, J.C.; Bodas-Salcedo, A.; Suzuki, K.; Gariel, P.; Haynes, J. Dreary state of precipitation in global models. *J. Geophys. Res. Atmos.* **2010**, *115*, D24. [[CrossRef](#)]
29. Kidd, C.; Levizzani, V. Status of satellite precipitation retrievals. *Hydrol. Earth Syst. Sci.* **2011**, *15*, 1109–1116. [[CrossRef](#)]
30. Tapiador, F.J.; Turk, F.J.; Petersen, W.; Hou, A.Y.; García-Ortega, E.; Machado, L.A.T.; Angelis, C.F.; Salio, P.; Kidd, C.; Huffman, G.J.; et al. Global precipitation measurement: Methods, datasets and applications. *Atmos. Res.* **2012**, *104*, 70–97. [[CrossRef](#)]
31. Sun, Q.; Miao, C.; Duan, Q.; Ashouri, H.; Sorooshian, S.; Hsu, K.L. A review of global precipitation data sets: Data sources, estimation, and intercomparisons. *Rev. Geophys.* **2018**, *56*, 79–107. [[CrossRef](#)]

32. Beck, H.E.; Vergopolan, N.; Pan, M.; Levizzani, V.; Dijk, A.I.J.M.; Weedon, G.P.; Brocca, L.; Pappenberger, F.; Huffman, G.J.; Wood, E.F. Global-scale evaluation of 22 precipitation datasets using gauge observations and hydrological modeling. *Satell. Precip. Meas.* **2020**, *2*, 625–653.
33. Xie, P.; Arkin, P.A. Global precipitation: A 17-year monthly analysis based on gauge observations, satellite estimates, and numerical model outputs. *Bull. Am. Meteorol. Soc.* **1997**, *78*, 2539–2558. [[CrossRef](#)]
34. Kidd, C. Satellite rainfall climatology: A review. *Int. J. Climatol.* **2001**, *21*, 1041–1066. [[CrossRef](#)]
35. Sturaro, G. A Closer look at the climatological discontinuities present in the NCEP/NCAR reanalysis temperature due to the introduction of satellite data. *Clim. Dyn.* **2003**, *21*, 309–316. [[CrossRef](#)]
36. Bengtsson, L.; Hagemann, S.; Hodges, K.I. Can climate trends be calculated from reanalysis data? *J. Geophys. Res.* **2004**, *109*, D11111. [[CrossRef](#)]
37. Kalnay, E.; Kanamitsu, M.; Kistler, R.; Collins, W.; Deaven, D.; Gandin, L.; Iredell, M.; Saha, S.; White, G.; Woollen, J.; et al. The NCEP/NCAR 40-year reanalysis project. *Bull. Am. Meteorol. Soc.* **1996**, *77*, 437–471. [[CrossRef](#)]
38. Kanamitsu, M.; Ebisuzaki, W.; Woolen, J.; Yang, S.K.; Hnilo, J.J.; Fiorino, M.; Potter, G.L. NCEP–DOE AMIP-II Reanalysis (R-2). *Bull. Am. Meteorol. Soc.* **2002**, *83*, 1631–1643. [[CrossRef](#)]
39. Uppala, S.M.; Kållberg, P.W.; Simmons, A.J.; Andrae, U.; Bechtold, V.D.C.; Fiorino, M.; Gibson, J.K.; Haseler, J.; Hernandez, A.; Kelly, G.A.; et al. The ERA-40 re-analysis. *Q. J. R. Meteorol. Soc.* **2005**, *131*, 2961–3012. [[CrossRef](#)]
40. Dee, D.P.; Uppala, S.M.; Simmons, A.J.; Berrisford, P.; Poli, P.; Kobayashi, S.; Andrae, U.; Balsameda, M.A.; Balsamo, G.; Bauer, P.; et al. The ERA-Interim reanalysis: Configuration and performance of the data assimilation system. *Q. J. R. Meteorol. Soc.* **2011**, *137*, 553–597. [[CrossRef](#)]
41. Hersbach, H.; Bell, B.; Berrisford, P.; Hirahara, S.; Horányi, A.; Muñoz-Sabater, J.; Nicolas, J.; Peubey, C.; Radu, R.; Schepers, D.; et al. The ERA5 global reanalysis. *Q. J. R. Meteorol. Soc.* **2020**, *146*, 1999–2049. [[CrossRef](#)]
42. Bell, B.; Hersbach, H.; Simmons, A.; Berrisford, P.; Dahlgren, P.; Horányi, A.; Muñoz-Sabater, J.; Nicolas, J.; Radu, R.; Schepers, D.; et al. The ERA5 global reanalysis: Preliminary extension to 1950. *Q. J. R. Meteorol. Soc.* **2021**, *147*, 4186–4227. [[CrossRef](#)]
43. Saha, S.; Moorthi, S.; Pan, H.L.; Wu, X.; Wang, J.; Nadiga, S.; Tripp, P.; Kistler, R.; Woollen, J.; Behringer, D.; et al. The NCEP climate forecast system reanalysis. *Bull. Am. Meteorol. Soc.* **2010**, *91*, 1015–1058. [[CrossRef](#)]
44. Saha, S.; Moorthi, S.; Wu, X.; Wang, J.; Nadiga, S.; Tripp, P.; Behringer, D.; Hou, Y.T.; Chuang, H.; Iredell, M.; et al. The NCEP climate forecast system version 2. *J. Clim.* **2014**, *27*, 2185–2208. [[CrossRef](#)]
45. Ebata, A.; Kobayashi, S.; Ota, Y.; Moriya, M.; Kumabe, R.; Onogi, K.; Harada, Y.; Yasui, S.; Miyaoka, K.; Takahashi, K.; et al. The Japanese 55-year Reanalysis “JRA-55”: An interim report. *SOLEA* **2011**, *7*, 149–152. [[CrossRef](#)]
46. Tashima, T.; Kubota, T.; Mega, T.; Ushio, T.; Oki, R. Precipitation Extremes Monitoring Using the Near-Real-Time GSMaP-GNRT6 Product. *IEEE J. Sel. Top. Appl. Earth Obs. Remote Sens.* **2020**, *13*, 5640–5651. [[CrossRef](#)]
47. Joyce, R.J.; Janowiak, J.E.; Arkin, P.A.; Xie, P. CMORPH: A method that produces global precipitation estimates from passive microwave and infrared data at high spatial and temporal resolution. *J. Hydrometeorol.* **2004**, *5*, 487–503. [[CrossRef](#)]
48. Huffman, G.J.; Bolvin, D.T.; Nelkin, E.J.; Wolff, D.B.; Adler, R.F.; Gu, G.; Hong, Y.; Bowman, K.P.; Stocker, E.F. The TRMM Multisatellite Precipitation Analysis (TMPA): Quasi-global, multiyear, combined-sensor precipitation estimates at fine scales. *J. Hydrometeorol.* **2007**, *8*, 38–55. [[CrossRef](#)]
49. Hong, Y.; Hsu, K.L.; Sorooshian, S.; Gao, X.G. Precipitation estimation from remotely sensed imagery using an artificial neural network cloud classification system. *J. Appl. Meteorol.* **2004**, *43*, 1834–1852. [[CrossRef](#)]
50. Hsu, K.L.; Gao, X.G.; Sorooshian, S.; Gupta, H.V. Precipitation estimation from remotely sensed information using artificial neural networks. *J. Appl. Meteorol.* **1997**, *36*, 1176–1190. [[CrossRef](#)]
51. Sorooshian, S.; Hsu, K.L.; Gao, X.; Gupta, H.V.; Imam, B.; Braithwaite, D. Evaluation of PERSIANN system satellite-based estimates of tropical rainfall. *Bull. Am. Meteorol. Soc.* **2000**, *81*, 2035–2046. [[CrossRef](#)]
52. Ushio, T.; Kachi, M. Kalman filtering applications for global satellite mapping of precipitation (GSMaP). In *Satellite Rainfall Applications for Surface Hydrology*; Gebremichael, M., Hossain, F., Eds.; Springer: New York, NY, USA, 2010; pp. 105–123.
53. Kubota, T.; Aonashi, K.; Ushio, T.; Shige, S.; Takayabu, Y.N.; Kachi, M.; Arai, Y.; Tashima, T.; Makaki, T.; Kawamoto, N.; et al. Global Satellite Mapping of Precipitation (GSMaP) products in the GPM era. *Satell. Precip. Meas.* **2020**, *1*, 355–373.
54. Herold, N.; Behrangi, A.; Alexander, L.V. Large uncertainties in observed daily precipitation extremes over land. *J. Geophys. Res. Atmos.* **2017**, *122*, 668–681. [[CrossRef](#)]
55. Sekaranom, A.B.; Masunaga, H. Origins of heavy precipitation biases in the TRMM PR and TMI products assessed with CloudSat and reanalysis data. *J. Appl. Meteorol. Climatol.* **2019**, *58*, 37–54. [[CrossRef](#)]
56. Masunaga, H.; Schröder, M.; Furuzawa, F.A.; Kummerow, C.; Rustemeier, E.; Schneider, U. Inter-product biases in global precipitation extremes. *Environ. Res. Lett.* **2019**, *14*, 125016. [[CrossRef](#)]
57. Hou, A.Y.; Kakar, R.K.; Neeck, S.; Azarbarzin, A.A.; Kummerow, C.D.; Kojima, M.; Oki, R.; Nakamura, K.; Iguchi, T. The global precipitation measurement mission. *Bull. Am. Meteorol. Soc.* **2014**, *95*, 701–722. [[CrossRef](#)]
58. Skofronick-Jackson, G.; Petersen, W.A.; Berg, W.; Kidd, C.; Stocker, E.F.; Krischbaum, D.B.; Kakar, R.; Braun, S.A.; Huffman, G.J.; Iguchi, T.; et al. The Global Precipitation Measurement (GPM) mission for science and society. *Bull. Am. Meteorol. Soc.* **2017**, *98*, 1679–1695. [[CrossRef](#)] [[PubMed](#)]

59. Setiawati, M.D.; Miura, F.; Aryastana, P. Validation of Hourly GSMaP and ground base estimates of precipitation for flood monitoring in Kumamoto, Japan. In *Geospatial Technology for Water Resource Applications*; CRC Press: Boca Raton, FL, USA, 2016; pp. 130–143.
60. Tian, Y.; Peters-Lidard, C.D.; Adler, R.F.; Kubota, T.; Ushio, T. Evaluation of GSMaP precipitation estimates over the contiguous United States. *J. Hydrometeorol.* **2010**, *11*, 566–574. [[CrossRef](#)]
61. Chen, Z.; Qin, Y.; Shen, Y.; Zhang, S. Evaluation of global satellite mapping of precipitation project daily precipitation estimates over the Chinese mainland. *Adv. Meteorol.* **2016**, *2016*, 9365294. [[CrossRef](#)]
62. Ning, S.; Song, F.; Udmale, P.; Jin, J.; Thapa, B.R.; Ishidaira, H. Error analysis and evaluation of the latest GSMaP and IMERG precipitation products over Eastern China. *Adv. Meteorol.* **2017**, *2017*, 1803492. [[CrossRef](#)]
63. Lu, D.; Yong, B. A preliminary assessment of the gauge-adjusted near-real-time GSMaP precipitation estimate over Mainland China. *Remote Sens.* **2020**, *12*, 141. [[CrossRef](#)]
64. Zhou, Z.; Guo, B.; Xing, W.; Zhou, J.; Xu, F.; Xu, Y. Comprehensive evaluation of latest GPM era IMERG and GSMaP precipitation products over mainland China. *Atmos. Res.* **2020**, *246*, 105132. [[CrossRef](#)]
65. Chua, Z.W.; Kuleshov, Y.; Watkins, A. Evaluation of satellite precipitation estimates over Australia. *Remote Sens.* **2020**, *12*, 678. [[CrossRef](#)]
66. Setiyoko, A.; Osawa, T.; Nuarsa, I.W. Evaluation of GSMaP precipitation estimates over Indonesia. *Int. J. Environ. Geosci.* **2019**, *3*, 26–43.
67. Kuleshov, Y.; Kurino, T.; Kubota, T.; Tashima, T.; Xie, P. WMO Space-Based Weather and Climate Extremes Monitoring Demonstration Project (SEMMP): First Outcomes of Regional Cooperation on Drought and Heavy Precipitation Monitoring for Australia and South-East Asia. Available online: <https://www.intechopen.com/books/rainfall-extremes-distribution-and-properties/wmo-space-based-weather-and-climate-extremes-monitoring-demonstration-project-semmp-first-outcomes-o> (accessed on 15 October 2023).
68. Zheng, D.; Yao, T.D. Research progress on formation and evolution of Qinghai-Tibet Plateau and its environmental and resource effects. *Chin. Basic Sci.* **2004**, *6*, 15–21. (In Chinese)
69. Ding, Y.; Chan, J.C.L. The East Asian summer monsoon: An overview. *Meteorol. Atmos. Phys.* **2005**, *89*, 117–142.
70. Shi, X.Y.; Shi, X.H. Climatological characteristics of summertime moisture budget over the southeast part of Tibetan Plateau with their impacts. *J. Appl. Meteorol. Sci.* **2008**, *19*, 41–46. (In Chinese)
71. Ding, Y.; Wang, Z. A study of rainy seasons in China. *Meteorol. Atmos. Phys.* **2008**, *100*, 121–138.
72. Immerzeel, W.W.; Beek, L.P.V.; Bierkens, M.F. Climate change will affect the Asian water towers. *Science* **2010**, *328*, 1382–1385. [[CrossRef](#)] [[PubMed](#)]
73. Chen, J.; Huang, W.; Jin, L.; Chen, J.; Chen, S.; Chen, F. A climatological northern boundary index for the East Asian summer monsoon and its interannual variability. *Sci. China Earth Sci.* **2018**, *61*, 13–22. [[CrossRef](#)]
74. Xu, X.D.; Dong, L.L.; Zhao, Y.; Wang, Y.J. Effects of the Asian Water Tower over the Qinghai-Tibet Plateau and the characteristics of atmospheric water circulation. *Chin. Sci. Bull.* **2019**, *64*, 2830–2841. (In Chinese)
75. Chen, J.; Huang, W.; Feng, S.; Zhang, Q.; Kuang, X.; Chen, J. The modulation of westerlies-monsoon interaction on climate over the monsoon boundary zone in East Asia. *Int. J. Climatol.* **2021**, *41*, 3049–3064. [[CrossRef](#)]
76. Hardy, R.L. Multiquadric equations of topography and other irregular surfaces. *J. Geophys. Res.* **1971**, *76*, 1905–1915. [[CrossRef](#)]
77. Fasshauer, G.E. *Meshfree Approximation Methods with MATLAB*; World Scientific Publishing Co., Inc.: Singapore, 2007; pp. 355–403.
78. Wu, J.; Zhang, L.; Zhao, D.; Tang, J. Impacts of warming and water vapor content on the decrease in light rain days during the warm season over eastern China. *Clim. Dyn.* **2015**, *45*, 1841–1857. [[CrossRef](#)]
79. Domroes, M.; Schaefer, D. Recent climate change affecting rainstorm occurrences: A case study in East China. *Clim. Past* **2008**, *4*, 303–309. [[CrossRef](#)]
80. Kubota, T.; Aonashi, K.; Ushio, T.; Shige, S.; Yamaji, M.; Yamamoto, M.; Hirose, H.; Takayabu, Y. A new version of Global Satellite Mapping of Precipitation (GSMaP) product released in December 2021. In Proceedings of the EGU General Assembly 2022, Vienna, Austria, 23–27 May 2022.
81. Kubota, T.; Shige, S.; Hashizume, H.; Aonashi, K.; Takahashi, N.; Seto, S.; Hirose, M.; Takayabu, Y.N.; Ushio, T.; Nakagawa, K.; et al. Global Precipitation Map Using Satellite-Borne Microwave Radiometers by the GSMaP Project: Production and Validation. *IEEE Trans. Geosci. Remote Sens.* **2007**, *45*, 2259–2275. [[CrossRef](#)]
82. Tustison, B.; Harris, D.; Foufoula-Georgiou, E. Scale issues in verification of precipitation forecasts. *J. Geophys. Res. Atmos.* **2001**, *106*, 11775–11784. [[CrossRef](#)]
83. Lv, X.; Guo, H.; Tian, Y.; Meng, X.; Bao, A.; De Maeyer, P. Evaluation of GSMaP Version 8 Precipitation Products on an Hourly Timescale over Mainland China. *Remote Sens.* **2024**, *16*, 210. [[CrossRef](#)]
84. Zhu, Z.; Yong, B.; Ke, L.; Wang, G.; Ren, L.; Chen, X. Tracing the error sources of global satellite mapping of precipitation for GPM (GPM-GSMaP) over the Tibetan Plateau, China. *IEEE J. Sel. Top. Appl. Earth Obs. Remote Sens.* **2018**, *11*, 2181–2191. [[CrossRef](#)]
85. Li, Q.; Wei, J.; Yin, J.; Qiao, Z.; Peng, W.; Peng, H. Multiscale comparative evaluation of the GPM and TRMM precipitation products against ground precipitation observations over Chinese Tibetan Plateau. *IEEE J. Sel. Top. Appl. Earth Obs. Remote Sens.* **2020**, *14*, 2295–2313. [[CrossRef](#)]

86. Jiang, Y.; Yang, K.; Li, X.; Zhang, W.; Shen, Y.; Chen, Y.; Li, X. Atmospheric simulation-based precipitation datasets outperform satellite-based products in closing basin-wide water budget in the eastern Tibetan Plateau. *Int. J. Climatol.* **2022**, *42*, 7252–7268. [[CrossRef](#)]
87. Song, Y.; Achberger, C.; Linderholm, H.W. Rain-season trends in precipitation and their effect in different climate regions of China during 1961–2008. *Environ. Res. Lett.* **2011**, *6*, 034025. [[CrossRef](#)]
88. Liu, B.; Chen, C.; Lian, Y.; Chen, J.; Chen, X. Long-term change of wet and dry climatic conditions in the southwest karst area of China. *Glob. Planet. Chang.* **2015**, *127*, 1–11. [[CrossRef](#)]
89. Shang, H.; Xu, M.; Zhao, F.; Tijjani, S.B. Spatial and temporal variations in precipitation amount, frequency, intensity, and persistence in China, 1973–2016. *J. Hydrometeorol.* **2019**, *20*, 2215–2227. [[CrossRef](#)]
90. Shawky, M.; Moussa, A.; Hassan, Q.K.; El-Sheimy, N. Performance assessment of sub-daily and daily precipitation estimates derived from GPM and GSMaP products over an arid environment. *Remote Sens.* **2019**, *11*, 2840. [[CrossRef](#)]
91. Lu, D.; Yong, B. Evaluation and hydrological utility of the latest GPM IMERG V5 and GSMaP V7 precipitation products over the Tibetan Plateau. *Remote Sens.* **2018**, *10*, 2022. [[CrossRef](#)]
92. Cohen Liechti, T.; Matos, J.P.; Boillat, J.L.; Schleiss, A.J. Comparison and evaluation of satellite derived precipitation products for hydrological modeling of the Zambezi River Basin. *Hydrol. Earth Syst. Sci.* **2012**, *16*, 489–500. [[CrossRef](#)]
93. Tang, G.; Clark, M.P.; Papalexiou, S.M.; Ma, Z.; Hong, Y. Have satellite precipitation products improved over last two decades? A comprehensive comparison of GPM IMERG with nine satellite and reanalysis datasets. *Remote Sens. Environ.* **2020**, *240*, 111697. [[CrossRef](#)]
94. Deng, P.; Zhang, M.; Guo, H.; Xu, C.; Bing, J.; Jia, J. Error analysis and correction of the daily GSMaP products over Hanjiang River Basin of China. *Atmos. Res.* **2018**, *214*, 121–134. [[CrossRef](#)]
95. Sun, G.; Wei, Y.; Wang, G.; Shi, R.; Chen, H.; Mo, C.; Rigo, T. Downscaling Correction and Hydrological Applicability of the Three Latest High-Resolution Satellite Precipitation Products (GPM, GSMaP, and MSWEP) in the Pingtang Catchment, China. *Adv. Meteorol.* **2022**, *2022*, 6507109. [[CrossRef](#)]

Disclaimer/Publisher’s Note: The statements, opinions and data contained in all publications are solely those of the individual author(s) and contributor(s) and not of MDPI and/or the editor(s). MDPI and/or the editor(s) disclaim responsibility for any injury to people or property resulting from any ideas, methods, instructions or products referred to in the content.